ISSN 1070-3284, Russian Journal of Coordination Chemistry, 2021, Vol. 47, No. 11, pp. 730–740. © Pleiades Publishing, Ltd., 2021.
Russian Text © The Author(s), 2021, published in Koordinatsionnaya Khimiya, 2021, Vol. 47, No. 11, pp. 668–678.

Effect of the Nature of Substituents in the Oxyacridine Ligands on the Luminescence Properties and Cytotoxicity of the Zinc Complexes

T. V. Balashova[a, *], S. K. Polyakova[a, b], A. A. Kukinov[a], R. V. Rumyantsev[a], G. K. Fukin[a], V. A. Ilichev[a], Yu. A. Gracheva[c], T. A. Antonenko[c], E. R. Milaeva[c], and M. N. Bochkarev[a, b]

[a] *Razuvaev Institute of Organometallic Chemistry, Russian Academy of Sciences, Nizhny Novgorod, Russia*

[b] *Lobachevskii State University, Nizhny Novgorod, Russia*

[c] *Moscow State University, Moscow, 119899 Russia*

**e-mail: petrovsk@iomc.ras.ru*

Received March 15, 2021; revised March 30, 2021; accepted April 1, 2021

Abstract—Zinc complexes with oxyacridine ligands ($Zn(Acr)_2$ and $[Zn(Acr)Et]_2$) are synthesized, and their structures are determined by X-ray structure analysis (CIF files CCDC nos. 2063229 and 2063230, respectively). The complexes exhibit a medium-intensity emission with maxima at 700 and 630 nm upon photoexcitation ($\lambda = 405$ nm). Both compounds also manifest weak electroluminescence properties. The complexes with methyl substituents in the ligands are the most luminescence-active of the whole series of the synthesized zinc compounds with the oxyacridine ligands $Zn(Acr^R)_2$ and $[Zn(Acr^R)Et]_2$ (R = Me, Br, H). The results of the MTT assay show a moderate cytotoxic activity of the synthesized compounds.

Keywords: 1,3-di-*tert*-butylacridin-4-ol, zinc, substituents, photoluminescence, electroluminescence, cytotoxicity, X-ray structure analysis

DOI: 10.1134/S1070328421100018

INTRODUCTION

In spite of numerous studies in the field of organic light-emitting diodes (OLED), the search for new efficient luminophores and studies of conversion energy processes are continued in many research centers [1–4]. The complexes of the main group metals with ligands of the oxyquinoline type found wide use as electroluminescent materials: Zn [5], Cd [6], Cu [7], and Al [8]. Among them, the zinc complexes attracted special attention due to high photo- and electroluminescence activities, high thermal stability, easy sublimation in vacuo, and a broad range of tunable electronic properties, which readily change upon the introduction of substituents in the ligands. In the series of the zinc-containing organic luminophores, the oxyquinolate complexes demonstrate the highest photoluminescence quantum yield [9]. 4-Hydroxyacridine can be presented as the 8-hydroxyquinoline derivative with the extended π system [10, 11], which assumes that this compound and related complexes have luminescence properties. The complexes of 4-hydroxyacridine with divalent cations, including Zn^{2+}, have already found use as emission components in the design of new OLED [12, 13]. In addition, acridines refer to the group of natural compounds with pronounced antibacterial and anticancer activities. The complexes of the acridine series manifest pharmacological activity as anticancer and antiparasitic drugs. It was expected that the introduction of alkyl substituents in the structures of the acridine ligands should increase the solubility of these compounds in organic solvents, which is required for their application in biomedicine and OLED technology [14, 15].

The synthesis and photophysical properties of the zinc complexes with sterically hindered 1,3-di-*tert*-butylacridin-4-ol are presented in this work. The energy levels of the highest occupied (HOMO) and lowest unoccupied (LUMO) molecular orbitals were calculated to take into account changes in the electronic structures. The effects of the substituents and structures of the synthesized compounds (Scheme 1) on the position of the luminescence maximum and luminescence intensity are discussed.

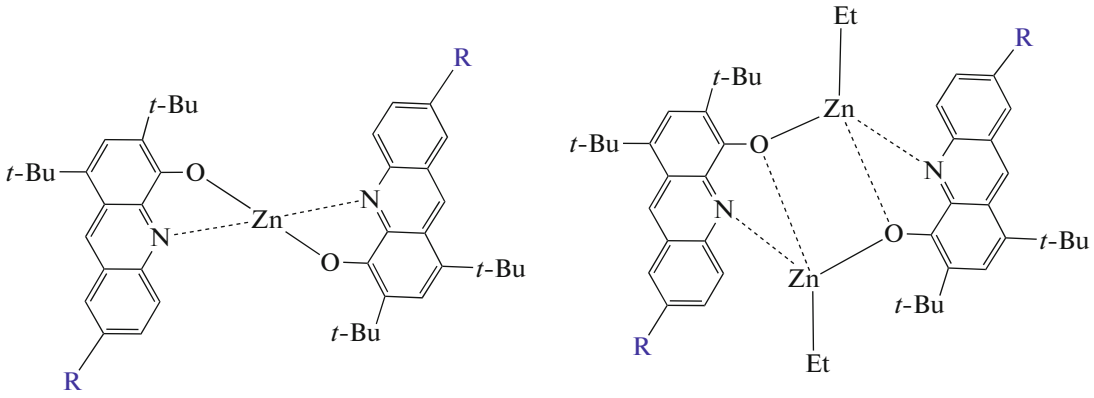

R = Me (**I**), Br (**III**), H (**V**) R = Me (**II**), Br (**IV**), H (**VI**)

Scheme 1.

EXPERIMENTAL

The syntheses were carried out under the conditions excluding contact with air oxygen and moisture using the standard Schlenk technique. Dimethoxyethane (DME) was dehydrated with sodium benzophenone ketyl, and pentane was dried over sodium using standard procedures and sampled in vacuo prior to use. Commercial reagent Et_2Zn (Aldrich) was used. The complexes $Zn(Acr^{Me})_2$ (**I**), $[Zn(Et)(Acr^{Me})]_2$ (**II**), $Zn(Acr^{Br})_2$ (**III**), and $[Zn(Et)(Acr^{Br})]_2$ (**IV**) were synthesized as described previously [16], and the 1,3-di-*tert*-butylacridin-4-ol ligand H(Acr) was synthesized using a known procedure [17].

Synthesis of $Zn(Acr)_2$ (V). A solution of diethylzinc (26 mg, 0.21 mmol) in DME (5 mL) was added to a solution of H(Acr) (129 mg, 0.42 mmol) in DME (10 mL). The reaction mixture was stirred at room temperature for 30 min. All volatiles were removed. The obtained substance was washed with cold pentane and dried in vacuo. The yield of complex **V** as a vinous powder was 113 mg (79%). The crystals suitable for X-ray diffraction analysis (XRD) were obtained by the recrystallization of complex **V** from a DME–diethyl ether (1 : 1) mixture of solvents.

For $C_{42}H_{48}N_2O_2Zn$

Anal. calcd., %	C, 74.38	H, 7.13	N, 4.13
Found, %	C, 74.31	H, 7.09	N, 4.20

IR (KBr), ν, cm^{-1}: 1622 m, 1589 w, 1577 s, 1558 m, 1514 s, 1438 s, 1408 m, 1373 m, 1344 s, 1306 m, 1280 m, 1253 m, 1239 m, 1219 m, 1199 w, 1146 m, 1104 m, 992 m, 975 w, 955 w, 941 m, 925 w, 895 w, 879 w, 849 w, 817 w, 764 s, 744 s, 645 m, 624 m, 600 w, 548 w, 531 m, 517 w, 505 w, 477 m. ^{1}H NMR (400 MHz pyridine-d_5), δ, ppm: 10.02 (d, J = 8.9 Hz, 1H), 9.59 (s, 1H), 8.18 (s, J = 8.3 Hz, 1H), 8.06 (s, 1H), 7.89–7.83 (m, 1H), 7.56–7.51 (m, 1H), 2.00 (s, 9H), 1.71 (s, 9H).

Synthesis of $[Zn(Et)(Acr)]_2$ (VI). A solution of diethylzinc (61 mg, 0.49 mmol) in DME (5 mL) was added to a solution of H(Acr) (135 mg, 0.41 mmol) in DME (10 mL). The reaction mixture was stirred at room temperature for 30 min. Orange crystals of complex **VI** precipitated during the slow removal of volatiles and the solvent. The yield was 160 mg (81%).

For $C_{46}H_{58}N_2O_2Zn_2$

Anal. calcd., %	C, 68.91	H, 7.29	N, 3.49
Found, %	C, 68.89	H, 7.35	N, 3.44

IR (KBr), ν, cm^{-1}: 1627 m, 1593 w, 1590 s, 1556 w, 1512 s, 1410 m, 1394 w, 1348 s, 1303 w, 1283 w, 1275 w, 1234 m, 1218 w, 1183 w, 1167 w, 1145 s,1095 m, 1026 w, 1009 w, 953 w, 939 w, 918 m, 893 w, 882 m, 846 w, 821 w, 764 s, 745 s, 701 w, 641 m, 629 m, 601 m, 593 w, 520 s, 476 w. ^{1}H NMR (400 MHz, pyridine-d_5), δ, ppm: 10.03 (d, J = 8.8 Hz, 1H), 9.60 (s, 1H), 8.19 (d, J = 8.2 Hz, 1H), 8.07 (s, 1H), 7.90–7.85 (m, 1H), 7.57–7.52 (m, 1H), 2.01 (s, 9H), 1.77 (t, J = 8.1 Hz, 3H), 1.72 (s, 9H), 1.32 (q, J = 8.2 Hz, 2H).

IR spectra were recorded on an FSM-1201 spectrometer in a range of 4000–400 cm^{-1} (suspensions in Nujol). The C,H,N,S elemental analyses were carried out on an Elementar Vario ELcube Analyzer instrument. Absorption spectra were recorded in a 1 cm quartz cell on a PerkinElmer Lambda-25 spectrometer in the range from 200 to 700 nm. Photoluminescence (PL) spectra were detected on a USB2000 spectrometer upon excitation with a diode laser at 405 nm. ^{1}H NMR spectra were recorded in C_5D_5N at 298 K on a Bruker Avance III 400 spectrometer with a working frequency of 400 MHz. The ^{1}H chemical shifts are presented relative to tetramethylsilane.

The three-layer OLED devices of the composition ITO/TPD/complex/Bath/Yb (ITO is indium–tin oxide (anode), TPD is *N*,*N*'-bis(3-methylphenyl)-*N*,*N*'-diphenylbenzidine (hole-transporting layer), Bath is 4,7-diphenyl-1,10-phenanthroline (hole-blocking layer), and Yb is cathode) were prepared by thermal depositon in a vacuum chamber at 10^{-6} Torr using a described procedure [18]. The thickness of the deposited layers was monitored with a quartz resonator.

Electroluminscence (EL) spectra in the visible range and voltage–current characteristics were detected on non-encapsulated samples using a USB-2000 fluorimeter (Ocean Optics), a PPE 3323 power source (GW Instek), and a GDM 8246 digital multimeter (GW Instek).

X-ray diffraction analysis (XRD) of complexes **V** and **VI** was carried out on Bruker D8 Quest and Oxford Xcalibur Eos automated diffractometers (graphite monochromator, MoK_α radiation, φ and ω scan modes, λ = 0.71073 Å), respectively. Experimental sets of intensities were integrated using the SAINT [19] (for **V**) and CrysAlisPro [20] (for **VI**) programs. Absorption corrections were applied using the SADABS software [21] (**V**) and SCALE3 ABSPACK algorithm [20] (**VI**). The structures were solved by the "dual-space" method using the SHELXT software [22]. All non-hydrogen atoms in complexes **V** and **VI** were refined by full-matrix least squares for F^2_{hkl} in the anisotropic approximation using the SHELXTL program package [23]. Hydrogen atoms were placed in the geometrically calculated positions and refined by the riding model (U_{iso}(H) = 1.5U_{equiv}(C) for CH_3 groups and U_{iso}(H) = 1.2U_{equiv}(C) for other groups). Selected crystallographic characteristics and XSA experimental parameters for complexes **V** and **VI** are presented in Table 1.

The structures were deposited with the Cambridge Crystallographic Data Centre (CIF files CCDC nos. 2063229 (**V**) and 2063230 (**VI**); ccdc.cam.ac.uk/structures/).

MTT assay. Cell viability was studied using MTT (3-(4,5-dimethylthiazol-2-yl)-2,5-diphenyltetrazolium bromide) assay by the Niks method with minor modifications [24]. The MCF-7 and HCT-116 lines of human cancer cells were cultivated in a DMEM medium (PanEko, Russia) with glutamine (PanEko, Russia) and antibiotics (PanEko, Russia) in CO_2 (5%) at 37°C. The compounds (20 mM) were dissolved in dimethyl sulfoxide (DMSO) and added to the medium for cell cultivation in the necessary concentration with a maximum DMSO content of 0.5 vol %. The control experiments showed that DMSO in these concentrations did not affect the cell viability. The cells were incubated in 96-well plates (7000 cells/well) and treated with the tested compounds and cisplatin at various concentrations (from 0.01 to 100 mM) at 37°C for 72 h. The cell viability was determined using the MTT assay, which quantitatively determines the activity of dehydrogenase. Then the cells were incubated at 37°C for 50 min with a solution of MTT (10 mL, 5 mg/mL) (SigmaAldrich, St. Louis, USA). The supernatant was rejected, and the cells were dissolved in DMSO (100 mL). The absorbance of the solution was measured at 570 nm using a 96-well plate (Anthos Zenyth 2000, Biochrom, Great Britain), and the percentage of the survived cells was calculated from the absorption of the untreated cells. Each experiment was repeated at least three times, and each concentration was tested three times. The values of 50% inhibition concentration (IC_{50}) with the standard deviation were calculated using the GraphPad Prism software (version 5.03).

RESULTS AND DISCUSSION

Complex **V** was synthesized by the reaction of diethylzinc and 1,3-di-*tert*-butylacridin-4-ol (Scheme 2). The reaction occurs easily at room temperature in DME to form dark vinous crystals of $Zn(Acr)_2$. When the reaction is carried out at a reactant ratio of 1 : 1 or in diethylzinc excess, then complex **VI** is formed as bright orange crystals. The synthesized compounds are highly soluble in the most part of organic solvents and stable in air both in the solid state and in solution.

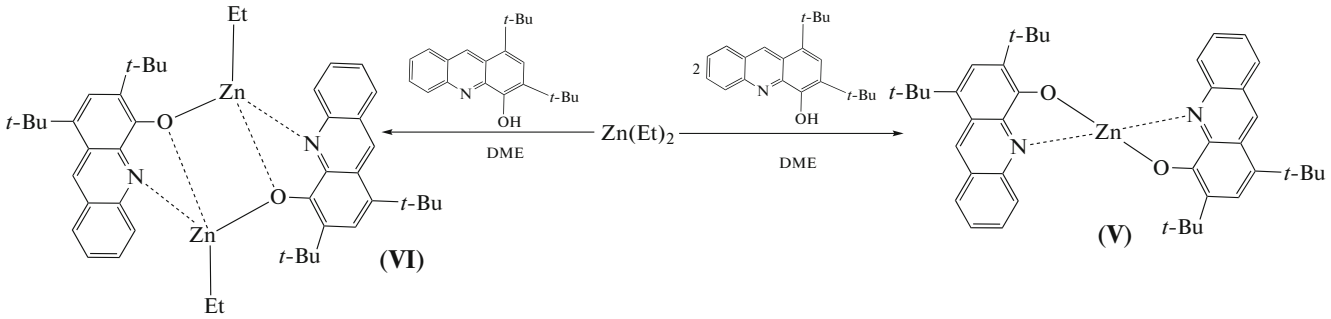

Scheme 2.

Table 1. Crystallographic data and experimental and structure refinement parameters for compounds **V** and **VI**

Parameter	Value	
	V	**VI**
Empirical formula	$C_{42}H_{48}N_2O_2Zn$	$C_{46}H_{58}N_2O_2Zn_2$
FW	678.19	801.68
Temperature, K	100(2)	100(2)
Crystal system	Monoclinic	Monoclinic
Space group	*C*2/*c*	*Pc*
a, Å	14.9598(6)	10.1326(3)
b, Å	17.4638(6)	13.9696(3)
c, Å	14.4507(5)	15.3811(5)
α, deg	90	90
β, deg	108.7204(12)	109.095(4)
γ, deg	90	90
V, Å^3	3575.6(2)	2057.38(11)
Z	4	2
ρ_{calc}, mg/m^3	1.260	1.294
μ, mm^{-1}	0.725	1.204
Crystal size, mm	0.19 × 0.17 × 0.04	0.51 × 0.22 × 0.10
F(000)	1440	848
θ, deg	2.649–26.022	2.916–25.023
Number of reflections collected/independent	24674/3533	28227/7246
R_{int}	0.0358	0.0490
R_1, wR_2 ($I > 2\sigma(I)$)	0.0353, 0.0795	0.0356, 0.0771
R_1, wR_2 (for all data)	0.0431, 0.0832	0.0466, 0.0822
Absolute structure parameter		–0.027(6)
S	1.052	1.033
Residual electron density (max/min), e/Å^3	0.347/–0.352	0.452/–0.262

According to the XSA data, complex **V** resembles in structure the related complex containing the methyl substituent in position 7 of the oxyacridine ligand [16]. The zinc cation is bound to two oxyacridine ligands coordinated via the bidentate mode (Fig. 1). Thus, the coordination environment of Zn^{2+} in complex **V** is a distorted tetrahedron ($\tau_4 = 0.73$) [25], and the coordination number is four.

The main geometric characteristics in complex **V** are in good agreement with the values published earlier for the related zinc compounds (coordination number 4) [16, 26, 27]. The Acr ligands in complex **V** are nearly planar. The mean deviation of the atoms from the plane is 0.03 Å. Interestingly, in the related compounds [16, 26, 27] the dihedral angle between the ligand planes varies from 86.90° to 88.45°, whereas this parameter is 75.41° in complex **V**. Probably, this mutual arrangement of the ligands in complex **V** is determined by the interactions between the ligands of the adjacent molecules. Infinite chains are formed in the crystal (Fig. 2). The planes of the ligands are parallel, and the distances between the centers of aromatic systems **A**...**B** and **C**...**D** are 3.486 Å. These geometric characteristics indicate the intermolecular π...π interaction between the oxyacridine ligands [28].

Complex **VI** is a nonsymmetric dimer (Fig. 3), whose molecular structure is close to those of the previously published related zinc complexes [16]. As in complex **V**, each zinc atom in complex **VI** has a distorted tetrahedral environment ($\tau_4 = 0.77$ and 0.75 for the Zn(1) and Zn(2) atoms, respectively [25]). The geometric characteristics of the oxyacridine ligands in complex **VI** are in good agreement with those for complex **V**. In turn, the Zn–O and Zn–N distances in complex **VI** are somewhat longer than those in complex **V**, which is consistent with the earlier published

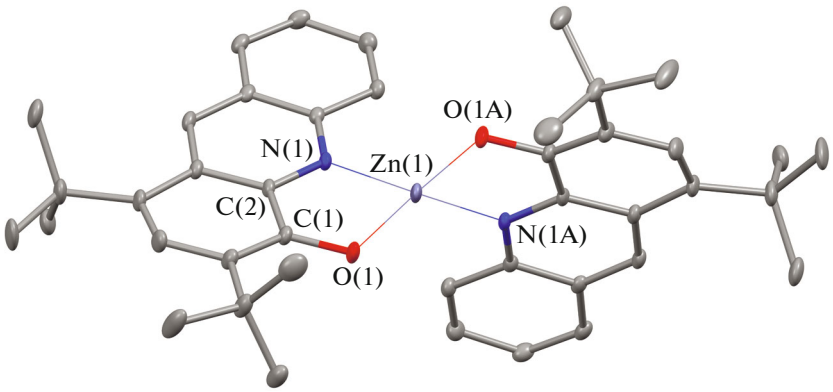

Fig. 1. Molecular structure of $Zn(Acr)_2$ (complex **V**). Thermal ellipsoids of 30% probability. Hydrogen atoms are omitted for clarity. Selected distances and angles in complex **V**: Zn(1)–O(1) 1.9315(13), Zn(1)–N(1) 2.0253(14), O(1)–C(1) 1.327(2), N(1)–C(2) 1.355(2), and C(1)–C(2) 1.445(3) Å and O(1)Zn(1)N(1) 84.07(6)°, O(1)Zn(1)O(1A) 114.46(8)°, O(1)Zn(1)N(1A) 128.51(6)°, N(1)Zn(1)O(1A) 128.51(6)°, and N(1)Zn(1)N(1A) 122.67(8)°.

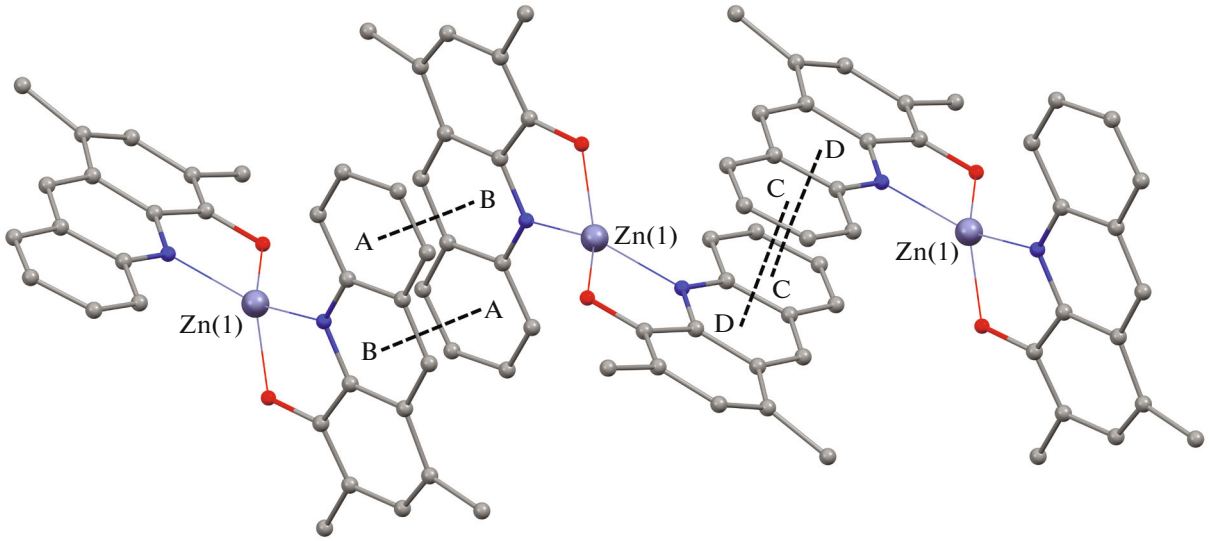

Fig. 2. Fragment of the crystal packing in complex **V**. Hydrogen atoms and methyl carbons of the *tert*-butyl groups are omitted for clarity.

data for the related dimeric zinc complexes [16, 29]. The ZnOZnO metallocycle in complex **VI** is nearly planar. The dihedral angle between the OZnO planes is 2.70°. This value better coincides with that for the zinc complex bearing the methyl substituent rather than with the complex having the bromine substituent in the oxyacridine ligand [16]. Unlike complex **V**, no intermolecular π...π interactions occur in the crystal of complex **VI**. However, in the molecule the ligand planes are arranged at an angle of 29.79° and the distance between the centers of the pyridine fragments is 3.651 Å (Fig. 3). These characteristics indicate that the intramolecular π...π interaction is possible [28].

The absorption spectra of solutions of complexes **V** and **VI** in acetonitrile at room temperature (Fig. 4) exhibit the intense band at 300 nm, the bands between 320 and 380 nm assigned to the π–π* transitions in the aromatic ligands, and also a broad band in a range of 510–535 nm that can be attributed to the ligand-to-metal charge-transfer transition. The introduction of the electron-donating substituent ($-CH_3$) in the aromatic ring results in a slight hypsochromic shift, and the electron-withdrawing substituent (–Br) induces the bathochromic shift in the absorption spectra (Fig. 4).

An efficient method for controlling the optical properties of metal complexes is the modification of the chelating ligand. It is known that the substituents in the quinoline ligand (depending on their nature and position in the ring) exert different effects on the fluorescence properties changing the radiation wavelength and intensity [9, 30]. A good correlation is observed

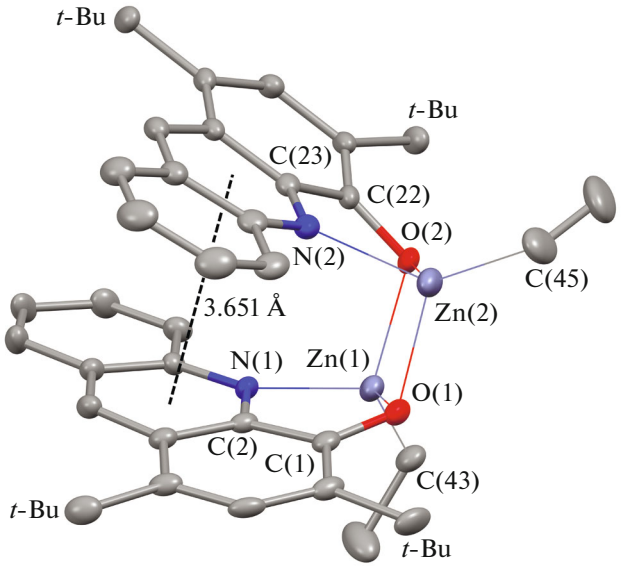

Fig. 3. Molecular structure of $[Zn(Acr)(Et)]_2$ (complex **VI**). Thermal ellipsoids of 30% probability. Hydrogen atoms are omitted for clarity. Selected distances and angles in complex **VI**: Zn(1)–O(1) 2.054(3), Zn(1)–O(2) 2.078(3), Zn(2)–O(1) 2.090(3), Zn(2)–O(2) 2.046(4), Zn(1)–N(1) 2.083(4), Zn(2)–N(2) 2.084(4), Zn(1)–C(43) 1.980(5), Zn(2)–C(45) 1.964(6), Zn(1)...Zn(2) 2.9663(8), O(1)–C(1) 1.348(6), O(2)–C(22) 1.353(6), N(1)–C(2) 1.343(6), N(2)–C(23) 1.350(6), C(1)–C(2) 1.435(7), and C(22)–C(23) 1.445(7) Å and O(1)-Zn(1)O(2) 88.31(14)°, O(1)Zn(1)N(1) 79.18(14)°, O(2)-Zn(1)N(1) 101.08(14)°, O(1)Zn(2)O(2) 88.19(14)°, O(2)-Zn(2)N(2) 79.76(15)°, N(2)Zn(2)O(1) 100.52(15)°, C(43)Zn(1)O(1) 126.65(18)°, C(43)Zn(1)O(2) 123.86(19)°, C(43)Zn(1)N(1) 125.2(2)°, C(45)Zn(2)O(1) 123.2(2)°, C(45)Zn(2)O(2) 119.7(2)°, and C(45)Zn(2)-N(2) 130.6(3)°.

between the electron-donor or electron-acceptor properties of the substituents and positions of band maxima in the luminescence spectra of the compounds [31]. It was shown for the zinc and aluminum oxyquinolinolate complexes that the introduction of the electron-donating groups in the pyridine ring or electron-withdrawing groups in the benzene ring would result in the blue shift of the radiation wavelength [32, 33]. As can be seen from Fig. 5, the introduction of the methyl substituent in position C-7 of the oxyacridine ligand substantially increases the PL intensity for both the $Zn(Acr^R)_2$ and $[Zn(Acr^R)(Et)]_2$ complexes (R = H, CH_3, Br) and simultaneously shifts the PL maximum to the short-wavelength range from 635 to 627 nm in the case of heteroligand complexes **VI** and **II** but exerts no effect on the spectra of homoligand complexes **V** and **I**. The introduction of the bromine substituent also affects the position of the maximum and luminescence intensity. For the $Zn(Acr^R)_2$ complexes, the PL maximum insignificantly shifts to the red spectral range from 690 to 705 nm, and the bathochromic shift of the PL maximum is 50 nm (from 635 to 685 nm) is observed for the $[Zn(Acr^R)(Et)]_2$ complexes. In both cases, the PL intensity decreases substantially. It should be mentioned that the PL intensity for heteroligand complexes **II**, **IV**, and **VI** is higher than that for the homoligand complexes. Of all synthesized compounds, the most intense PL is observed for heteroligand complex **II** with the methyl substituents in the oxyacridine ligands, which is associated, most likely, with specific features of the structure of the crystalline lattices of the synthesized compounds.

The DFT calculations of isolated molecules of compounds **V** and **VI** were performed using the B3LYP functional and full-electron 6-31G** basis set to evaluate the influence of methyl and bromine substituents on the electronic structures of the zinc acridinolate complexes. It should be mentioned that the chosen calculation level adequately reproduces the geometric parameters of these molecules in the crystal. The difference in bond lengths in the coordination sphere of the zinc atoms does not exceed 0.02 and 0.03 Å for complexes **V** and **VI**, respectively. The quantum-chemical calculations for complexes **I**–**IV** were made earlier [16]. The energies of the molecular orbitals of the $Zn(Acr^R)_2$ and $[Zn(Acr^R)(Et)]_2$ (R = H, CH_3, Br) compounds are presented in Table 2.

The HOMO and LUMO in complexes **V** and **VI** are mainly localized on the aromatic rings (Fig. 6). The LUMO in compound **VI** represents the orbital of the pure oxyacridine ligand without a metal atom contribution. On going to the HOMO, the contribution of the wave functions of each zinc atom increases to 4%. In complex **V**, a low contribution of the Zn atom (~1%) is observed in both the HOMO and LUMO orbitals. Therefore, the HOMO–LUMO electronic

Table 2. Energies of the molecular orbitals in complexes **I**–**VI**

Orbital	Complex					
	I	**II**	**III**	**IV**	**V**	**VI**
	eV					
HOMO	–4.79	–4.97	–4.68	–5.20	–4.85	–5.02
LUMO	–2.13	–2.45	–2.16	–2.59	–2.22	–2.33
HOMO–LUMO	2.66	2.72	2.52	2.61	2.63	2.68

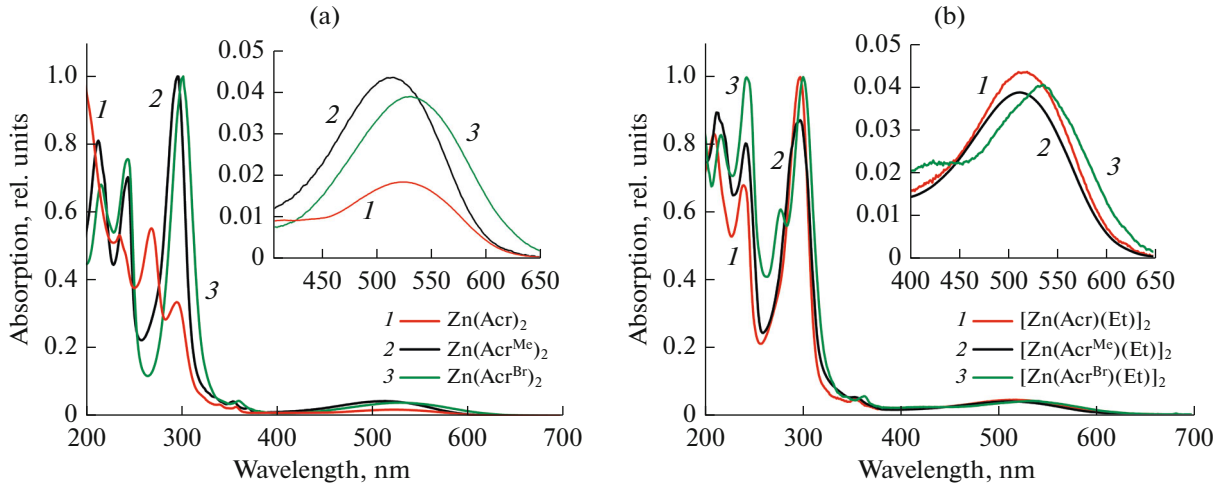

Fig. 4. Absorption spectra of the Zn complexes: (a) **I**, **III**, and **V** and (b) **II**, **IV**, and **VI** in a CH_3CN solution (2×10^{-5} M).

transitions can be considered as the interligand charge transfer with an insignificant contribution of the metal-to-ligand charge transfer.

As can be shown for the Al and Zn 8-oxyquinolinolate complexes [2, 30], the introduction of the electron-donating substituents ($-CH_3$) in the pyridine ring of the ligand results in an insignificant hypsochromic shift in the absorption and luminescence spectra. A similar situation is observed for our complexes. The introduction of the bromine atom in position C-7 of the oxyacridine ligand decreases the HOMO/LUMO forbidden band gap. Owing to this, the PL maxima in the spectra of zinc complexes **III** and **IV** are shifted to the red range relative to complexes **V** and **VI** without methyl and bromine substituents in the ligands (Fig. 5).

The EL properties of complexes **V** and **VI** were studied for the three-layer OLED devices of the ITO/TPD (25 nm)/complex (45 nm)/BATH (15 nm)/LiF (0.5)/Al configuration. Both devices exhibited EL although with a low intensity (Fig. 7).

An increase in the HOMO/LUMO forbidden band gap for complex **VI** results in the hypsochromic shift in the EL spectrum compared to complex **V**. The voltage–luminosity and voltage–current characteristics of the considered devices are presented in Fig. 8. Their operating characteristics are given in Table 3. The efficiency of the devices based on complexes **V** and **VI** turned out to be lower than that of earlier studied complexes **I** and **II** with methyl substituents in the ligands: the turn-on voltage was 9–10 V, the maximum luminous intensity was 15–16 cd/m^2 at 30 V, and the current efficiency was 0.020–0.23 cd/A [16]. The devices based on complexes **III** and **IV** containing the brominated ligands exhibited no luminescence even at a high voltage [16]. The position and shape of the bands in the EL spectra (Fig. 7) of complexes **V** and **VI** are the same as those in the corresponding PL spectra. As in the PL spectra, the relative intensity of the EL spectra of complex **VI** is higher by a factor of 2 than that of complex **V**.

As can be seen from Table 2, the introduction of ethyl ligands in the zinc complexes substantially changes the values of the LUMO and HOMO. It can be assumed that the higher values of the LUMO and HOMO lead to the retention of holes and electrons in the organic light-emitting layer thus enhancing the efficiency of electron-hole recombination. Owing to the structures of complexes **II** and **VI**, the mobility of electrons increases and the probability of internal electronic transitions decreases and, hence, the corresponding zinc complexes are characterized by the better luminescence properties compared to compounds **I** and **V**.

Table 3. Operating characteristics of the ITO/TPD/complex/BATH/LiF/Al diodes*

Complex	η_i, cd A^{-1}	η_p, lm W^{-1}	U, V**	Maximum luminous intensity, cd/m^2
$Zn(Acr)_2$	0.83 (20 V)	0.26 (20 V)	11	1.5 (30 V)
$[Zn(Acr)(Et)]_2$	3.15 (18 V)	1.1 (18 V)	6	2.5 (30 V)

* η_i is the current efficiency, η_p is the power efficiency, and U is the operating voltage.
** At a luminous intensity of 0.1 cd/m^2.

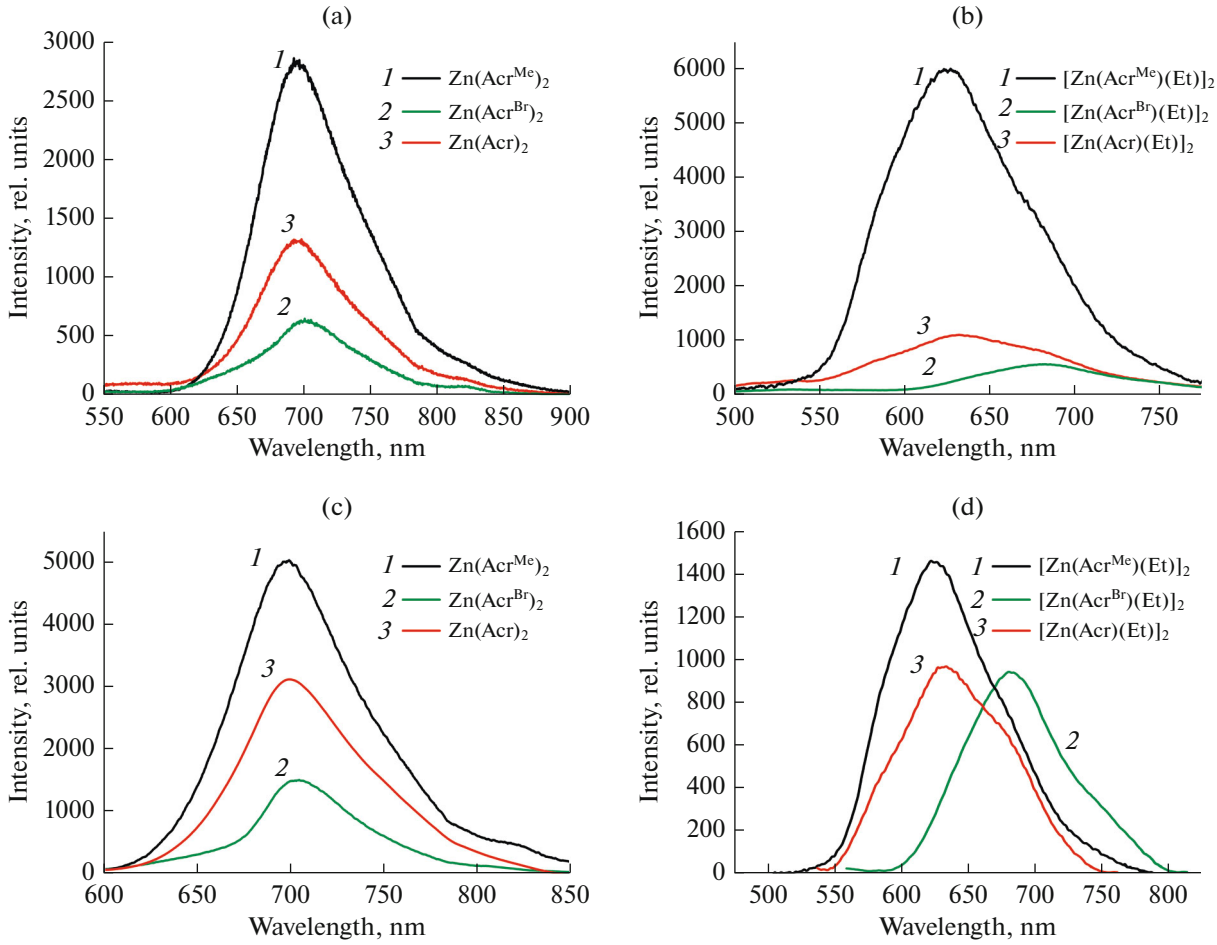

Fig. 5. Photoluminescence spectra of the solid samples of complexes (a, c) **I**, **III**, and **V** at λ_{exc} = (a) 365 and (c) 405 nm and (b, d) **II**, **IV**, and **VI** at λ_{exc} = (b) 365 and (d) 405 nm at room temperature.

Many enzymes present in the living organism contain zinc. It is known that the zinc complexes are characterized by a broad range of biological activity, in particular, antimicrobial and anticancer activities [34–36]. Increasing interest in the metal complexes based on the heterocyclic aromatic ligands is observed in the recent years, since they are significant for biochemistry [37]. Therefore, 4-hydroxyacridine attracts attention due to its pharmacological properties [38]. It was proved that 4-hydroxyacridine is an excellent chelating and intercalating ligand. The Ni(II) [11] and Pd(II) [39] complexes based on 4-hydroxyacridine turned out to be promising from the viewpoint of biological activity, particularly, anticancer activity.

Zinc(II) complexes **I**–**V** were tested to cytotoxicity toward the human cancer cell lines. The cytotoxicity of the compounds in vitro was estimated on the HCT-116 (human colon cancer) and MCF-7 (human mammary adenocarcinoma) lines. The activity of the compounds was compared to the effect of cisplatin. The results of the study showed that complex **V** was the most active, whereas compounds **I**–**IV** are characterized by a moderate cytotoxicity, which is probably related to the effect of the nature of the substituents in the oxyacridine ligands (Table 4).

To conclude, the zinc oxyacridinolate complexes $Zn(Acr)_2$ and $[Zn(Acr)Et]_2$ were synthesized, and their structures were determined by XSA. Their luminescence properties were studied. The compounds exhibited a medium-intensity emission with maxima at 700 and 630 nm upon photoexhitation (λ = 405 nm). Both complexes also manifested weak electroluminescence properties. Of the whole series of synthesized zinc compounds **I**–**VI**, the complexes with methyl substituents in the oxyacridine ligands (**I** and **II**) turned out to be most luminescence-active. The DFT calculations of the isolated molecules were performed to evaluate the influence of methyl and bromine substituents on the electronic structures of zinc acridinolates. The introduction of the electron-donating substituents ($-CH_3$) in the pyridine ring of the ligand results in an insignificant hypsochromic shift in the absorption and luminescence spectra. The introduction of the bromine atom leads to a decrease

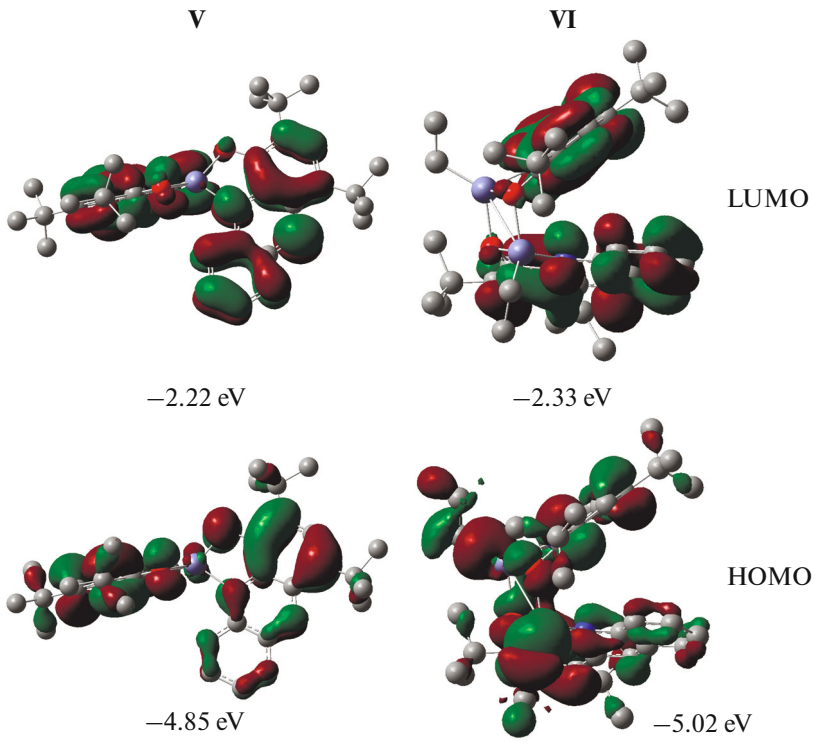

Fig. 6. The B3LYP/6-31G** isosurfaces of the HOMO and LUMO orbitals for complexes **V** and **VI** (0.02 a.u.). Hydrogen atoms are omitted.

in the HOMO/LUMO forbidden band gap and to a red shift of the PL maximum in the spectra of the zinc complexes. The MTT assay was carried out to study biological activity, and its results showed a weak cytotoxic activity of the synthesized zinc complexes. Compound **V** having neither methyl, nor bromine substituents in the ligands turned out to be most active.

ACKNOWLEDGMENTS

The studies were carried out using equipment of the Center for Collective Use "Analytical Center of Institute of Organometallic Chemistry of Russian Academy of Sciences." The XSA studies of complexes **V** and **VI** were carried out in terms of state assignment of the Institute of Organometallic Chemistry (Russian Academy of Sciences).

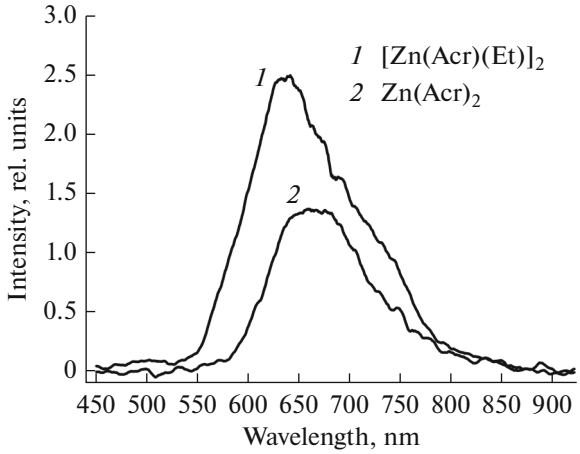

Fig. 7. Electroluminescence spectra of complexes (*2*) **V** and (*1*) **VI**.

Table 4. The values of IC_{50} (μM) for complexes **I**–**V** and cisplatin toward the HCT-116 and MCF-7 cell lines in the MTT assay

Compound	HCT-116	MCF-7
$Zn(Acr^{Me})_2$ (**I**)	147 ± 12	121 ± 11
$[Zn(Et)(Acr^{Me})]_2$ (**II**)	43 ± 5	54 ± 10
$Zn(Acr^{Br})_2$ (**III**)	85 ± 7	107 ± 11
$[Zn(Et)(Acr^{Br})]_2$ (**IV**)	121 ± 11	116 ± 10
$Zn(Acr)_2$ (**V**)	25 ± 5	31 ± 5
Cisplatin	7 ± 4	15 ± 3

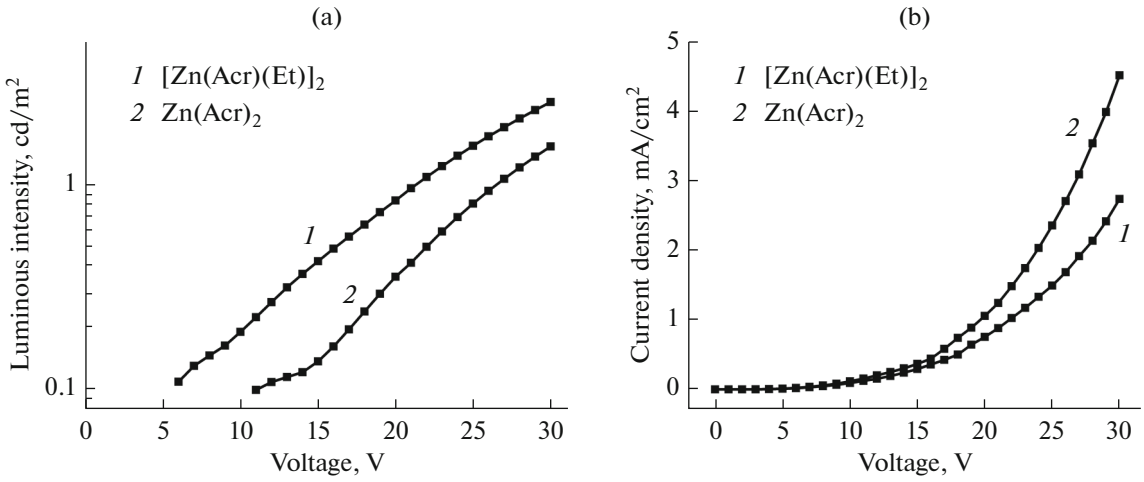

Fig. 8. (a) Voltage–luminosity and (b) voltage–current characteristics of the OLED based on complexes (*2*) **V** and (*1*) **VI**.

FUNDING

This work was supported by the Russian Science Foundation, project no. 20-73-10115.

CONFLICT OF INTEREST

The authors declare that they have no conflicts of interest.

REFERENCES

1. Mitschke, U. and Bauerle, P., *J. Mater. Chem.*, 2000, vol. 10, p. 1471.
2. Chen, C.H. and Shi, J., *Coord. Chem. Rev.*, 1998, vol. 171, p. 161.
3. Bunzli, J.-C.G. and Piguet, C., *Chem. Soc. Rev.*, 2005, vol. 34, p. 1048.
4. De Sa, G.F., Malta, O.L., and De Mello Donega, C., *Coord. Chem. Rev.*, 2000, vol. 196, p. 165.
5. Ghedini, M., Deda, M.L., Aiello, I., and Grisolia, A., *Inorg. Chim. Acta*, 2004, vol. 357, p. 33.
6. Wang, H., Wang, W.S., and Zhang, H.S., *Talanta*, 2001, vol. 53, p. 1015.
7. Wei, L.-J., Gao, H.-L., and Cui, J.-Z., *Phosphorus, Sulfur Silicon Relat. Elem.*, 2012, vol. 187, p. 1101.
8. Mishra, A., Nayak, P.K., and Periasamy, N., *Tetrahedron Lett.*, 2004, vol. 45, p. 6265.
9. Jianbo, H., Tingting, Z., Yongjing, C., et al., *J. Fluoresc.*, 2018, vol. 28, no. 5, p. 1121.
10. Mastropietro, T.F., Szerb, E.I., Deda, M.L., et al., *Eur. J. Inorg. Chem.*, 2013, vol. 2013, p. 2188.
11. Crispini, A., Pucci, D., Sessa, S., et al., *New J. Chem.*, 2003, vol. 27, p. 1497.
12. Hamada, J., Sano, K., Fujita, M., et al., *Jpn. Kokai Tokkyo Koho*, 1995, JP 07166159 A 19950627.
13. Cui, Z., Li, X., Li, L., et al., *Bioorg. Med. Chem.*, 2016, vol. 24, p. 261.
14. Kumar, A., Kumar, N., Roy, P., et al., *Med. Chem. Res.*, 2015, vol. 24, p. 3272.
15. Balashova, T.V., Arsenyev, M.V., Polyakova, S.K., et al., *J. Mol. Struct.*, 2021, vol. 1229, p. 129798.
16. Polyakova, S.K., Balashova, T.V., Rumyantcev, R.V., et al., *Mendeleev Commun.*, 2021, vol. 31, p. 262.
17. Katkova, M.A., Pushkarev, A.P., Balashova, T.V., et al., *J. Mater. Chem.*, 2011, vol. 21, p. 16611.
18. *SAINT. Data Reduction and Correction Program*, Madison: Bruker AXS., 2014.

19. *Rigaku Oxford Diffraction. CrysAlis Pro Software System. Version 1.171.40.84a*, Wroclaw: Rigaku Corporation, 2020.
20. Krause, L., Herbst-Irmer, R., Sheldrick, G.M., and Stalke, D., *J. Appl. Crystallogr.*, 2015, vol. 48, no. 1, p. 3.
21. Sheldrick, G.M., *Acta Crystallogr., Sect. A: Found. Adv.*, 2015, vol. 71, no. 1, p. 3.
22. Sheldrick, G.M., *Acta Crystallogr., Sect. C: Struct. Chem.*, 2015, vol. 71, p. 3.
23. Niks, M. and Otto, M., *J. Immunol. Methods*, 1990, vol. 130, p. 149.
24. Yang, L., Powell, D.R., and Houser, R.P., *Dalton Trans.*, 2007, no. 9, p. 955.
25. Wang, D., Li, S.-M., Zheng, J.-Q., et al., *Inorg. Chem.*, 2017, vol. 56, p. 984.
26. Czugler, M., Neumann, R., and Weber, E., *Inorg. Chim. Acta*, 2001, vol. 313, p. 100.
27. Janiak, C., *Dalton Trans.*, 2000, no. 21, p. 3885.
28. Bakewell, C., Fateh-Iravani, G., Beh, D.W., et al., *Dalton Trans.*, 2015, vol. 44, p. 12326.
29. Pérez-Bolvar, C., Montes, V.A., and Anzenbacher, P., *Inorg. Chem.*, 2006, vol. 45, p. 9610.
30. Fazaeli, Y., Amini, M.M., Najafi, E., et al., *J. Fluoresc.*, 2012, vol. 22, p. 1263.
31. Sapochak, L.S., Padmaperuma, A., Washton, N., et al., *J. Am. Chem. Soc.*, 2001, vol. 123, p. 6300.
32. Kido, J. and Iizumi, Y., *Chem. Lett.*, 1997, vol. 10, p. 963.
33. Zhu, T., Wang, Y., Ding, W., et al., *Chem. Biol. Drug Des.*, 2015, vol. 85, p. 385.
34. Li, Y., Yang, Z., Zhou, M., et al., *J. Mol. Struct.*, 2017, vol. 1130, p. 818.
35. Sankarganesh, M., Dhaveethu Raja, J., Adwin Jose, P.R., et al., *J. Fluoresc.*, 2018, vol. 28, no. 4, p. 975.
36. Oehninger, L., Rubbiania, R., and Ott, I., *Dalton Trans.*, 2013, vol. 42, p. 3269.
37. Matsumura, K., *J. Am. Chem. Soc.*, 1927, vol. 49, p. 810.
38. Pucci, D., Albertini, V., Bloise, R., et al., *J. Inorg. Biochem.*, 2006, vol. 100, p. 1575.

Translated by E. Yablonskaya